European Polymer Journal 210 (2024) 112954

Contents lists available at ScienceDirect

European Polymer Journal

journal homepage: www.elsevier.com/locate/europolj

Luminescent hollow spherical nanoparticles with enhanced imaging contrast through hydrogen bonding connected micelles

Tzu-Ling Ma [a], Wei-Ting Du [a], Mohamed Gamal Mohamed [a], Shiao-Wei Kuo [a,b,*]

[a] Department of Materials and Optoelectronic Science, Center of Crystal Research, National Sun Yat-Sen University, Kaohsiung 804, Taiwan
[b] Department of Medicinal and Applied Chemistry, Kaohsiung Medical University, Kaohsiung 807, Taiwan

ARTICLE INFO

Keywords:
Hydrogen Bonding
Micelles
Triphenylamine
Aggregation Enhanced Emission
Hollow Sphere

ABSTRACT

Herein, we propose an innovative method for synthesizing luminescent hollow spherical nanoparticles. Our method involves the construction of hydrogen bonding connected micelles (HBCMs) utilizing inter-polymer complexes of poly(styrene-*alt*-hydroxyphenylmaleimide)/poly(4-vinylpyridine) (poly(S-*alt*-HPMI)/P4VP), which could undergo self-assembly, resulting in the formation of core/shell nanostructures in the selective solvent. The aim was to incorporate two types of fluorescent compounds, namely tris(4–bromophenyl)amine (TPA–Br_3) and 1,1,2,2–tetrakis(4–bromophenyl)ethene (TPE–Br_4), as the cross-linkers to enhance the shell structures of HBCMs and using dimethylformamide (DMF) was employed to remove the core structures, aiming to pursue the formation of luminescent hollow spheres. Transmission electron microscopy (TEM) images confirmed the formation of self-assembled spherical structures formed by poly(S-*alt*-HPMI)/P4VP inter-polymer complexes. The morphological features, hydrogen bonding interactions, particle sizes, cross-linking reactions, core removal, and thermal properties were thoroughly investigated by TEM, atomic force microscope (AFM), dynamic light scattering (DLS) instrument, Fourier transform infrared (FTIR) spectroscopy, ^{1}H nuclear magnetic resonance (NMR) spectroscopy, thermogravimetric analysis (TGA), and differential scanning calorimetry (DSC) analyses. Moreover, the optical properties were also explored by fluorescence microscope and photoluminescence (PL). This evidence indicates that the HBCMs could be directly cross-linked with TPA–Br_3 or TPE–Br_4 and subsequently transformed into hollow spheres by the addition of DMF. Fluorescent particles featuring hollow spheres could be prepared successfully without traditional dye staining or labeling. This advancement holds promising potential for applications in nano-carriers with improved imaging contrast.

1. Introduction

Over several decades, various research efforts have focused on the development of self-assembling polymeric micelles, which are constructed using diverse types of copolymers, such as amphiphilic diblock copolymers [1–3], graft copolymers [4–6], or ionic copolymers [7–9]. Upon reaching the critical micelles concentration (CMC), these covalently bonded copolymers would aggregate to form well-defined ordered structures [10]. The appeal of polymeric micelles lies in the nanoscale particle dimensions, leading to extensive studies of nano-carriers, electrolytes, and templates [11–16]. Currently, a predominant focus is on the design of degradable amphiphilic diblock copolymers for therapeutic applications. However, challenges persist, including environmental circumstances (such as solvent, temperature, and pH), the threshold of CMC, and the drug loading efficiency, which need to pose challenges of *in vitro* studies [17–19].

In response to the complicated synthesis and limitations of these copolymers, a more innovative and practical approach termed the "block-copolymer-free" strategy, has been explored. This approach involves the formation of noncovalently connected micelles (NCCMs) composing complementary polymer pairs containing hydrogen bonding donor and acceptor moieties. These polymer pairs are introduced into the selective solvent, leading to the formation of core/shell structures inter-connected by intermolecular hydrogen bonding [20] or host–guest interactions. For example, the self-assembly behavior occurred when PtBA-ADA homopolymer and PGMA-CD diblock copolymer were both introduced in water, which resulted in the core/shell structure, primarily induced by the physically host–guest interaction between β-CD and ADA portion [21]. Our previous study demonstrated that thymine-functionalized PVBT/adenine-terminated PEO-A homopolymers would

* Corresponding author.
E-mail address: kuosw@faculty.nsysu.edu.tw (S.-W. Kuo).

https://doi.org/10.1016/j.eurpolymj.2024.112954
Received 30 January 2024; Received in revised form 14 March 2024; Accepted 17 March 2024
Available online 26 March 2024

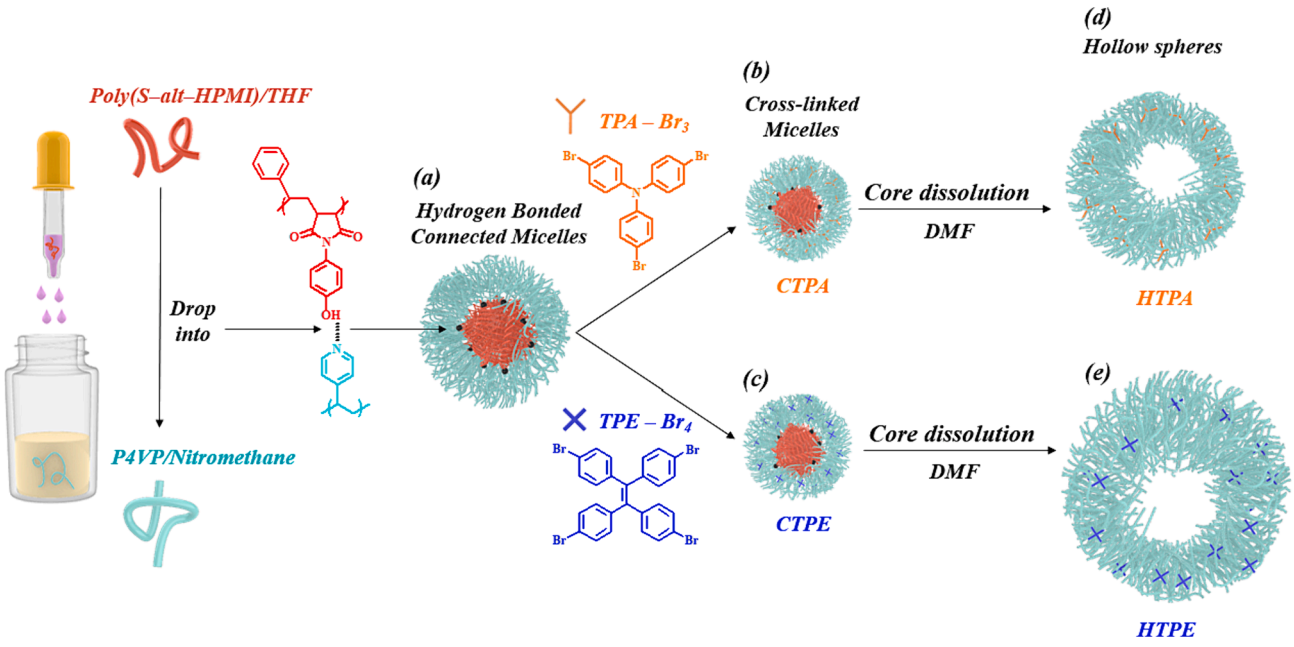

Scheme 1. Construction of (a) hydrogen-bonded connected micelles (HBCMs) from poly(S-*alt*-HPMI)/P4VP complex, crosslinked micelles with TPA–Br_3 (b) and TPE–Br_4 (c), hollow spheres dissolution in the DMF transform from CTPA (d), and CTPE (e).

self-assemble into the "graft-like" copolymers in DMF. This assembly was driven by complementary multiple hydrogen bonding interactions between PEO-A and PVBT fragments then formed the core/shell structures in a selective water environment [22]. Furthermore, Jiang *et al.* reported that with an increase in the hydrogen bonding donor, there was a corresponding rise in the density of the hydrogen bonding interaction site at the core/sell interface, ultimately resulting in the formation of a rod-like structure rather than a spherical structure [23]. In our previous study, we were interested in the decrease of hydrogen bonding acceptor and transformed copolymer sequences to mediate the hydrogen bonding interaction site at the core/sell interface, which also achieved similar results [24]. Another attraction of NCCMs is that it is simple to achieve a hollow structure by changing solvent at ambient temperature without using non-environmentally friendly calcination or chemical etching [25,26]. It may become a promising strategy to potentially replace the current approaches aimed at pursuing vesicle structures in the chemotherapeutic field to overcome challenges in drug delivery [27].

In the field of bioimaging, organic fluorophores play a crucial role, finding applications through their covalent integration into block copolymer micelles. These fluorophores serve as fluorescent labels, enabling the monitoring of the movement of micelles within living cells, and facilitating targeted drug delivery [28]. For example, the previous work reported the use of amine-functionalized poly(St-*co*-MAh) labeling as a green dye [29] and Razzaque *et al.* demonstrated blue fluorescence in Py-HMOCs-FA by confocal microscopy [30]. Within our group, we have synthesized numerous conjugated microporous polymers (CMPs) based on triphenylamine (TPA) or tetraphenylethylene (TPE) with π-conjugated skeleton structures, which are widely applied in photocatalysis, phototherapy, and bioimaging [31–34] In this context, aggregation-induced emission (AIE) fluorophores, particularly the well-known TPE, have emerged as a preferred choice for applications in drug delivery and bioimaging [26,35,36].

In this study, we explored two different kinds of fluorescent compounds, TPA–Br_3 and TPE–Br_4, as cross-linkers to stabilize the micelles structures, which had not previously reported the role in stabilizing micelles. Our study involved constructing hydrogen bonding-connected micelles (HBCMs) based on the poly(S-*alt*-HPMI) alternating copolymer/P4VP homopolymer, which is self-assembled driven by weak intermolecular hydrogen as described in our previous study [24]. To improve the structural stability of P4VP, we introduced cross-linking agents TPA–Br_3 or TPE–Br_4, resulting in the formation of HBCMs. By carefully manipulating the solvent, the hollow structures were achieved by medicating the chemical structures, cross-linking reaction, hollow nature, and thermal stability of poly(S-*alt*-HPMI)/P4VP hydrogen bonding connected micelle by FTIR, ^{1}H NMR, TGA, DLS, and TEM analyses. We also used a fluorescence microscope and photoluminescence to confirm the fluorescent properties of nanoparticles without the additional dye staining or labeling. The results revealed that the hydrogen bonding connected micelles, cross-liked with TPA–Br_3 or TPE–Br_4 and subsequently transformed into hollow spheres, display the potential applications as nanocarrier with imaging contrast capabilities.

2. Experimental section

2.1. Materials

Nitromethane (98 %) was purchased from Alfa Aesar. Tetrahydrofuran (THF) and *N*, *N*–dimethylformamide (DMF) were obtained from Acros Organics. All the solvents were used as received without further purification. Poly(styrene–*alt*–hydroxyphenylmaleimide) [poly (S–*alt*–HPMI)] alternating copolymer [37], poly(4–vinylpyridine) (P4VP) homopolymer [38], TPA–Br_3 and TPE–Br_4 [39] were synthesized previously in our previous studies.

2.2. Preparation of poly(S–alt–HPMI)/P4VP hydrogen bonding connected micelles (HBCMs)

For preparing the micelles in the selective solvent, poly (S–*alt*–HPMI)/THF solution (8 mg/2 mL) was added slowly over a period of about 10 min to P4VP/nitromethane solution (3.6 mg/ 18 mL) in a 20 mL vial bottle. The mixing solution transformed from colorless to canary yellow, implying the construction of micelles. This resulting mixture was stirred at room temperature overnight and then stable for 2 weeks before conducting further measurements (Scheme 1(a)) [24].

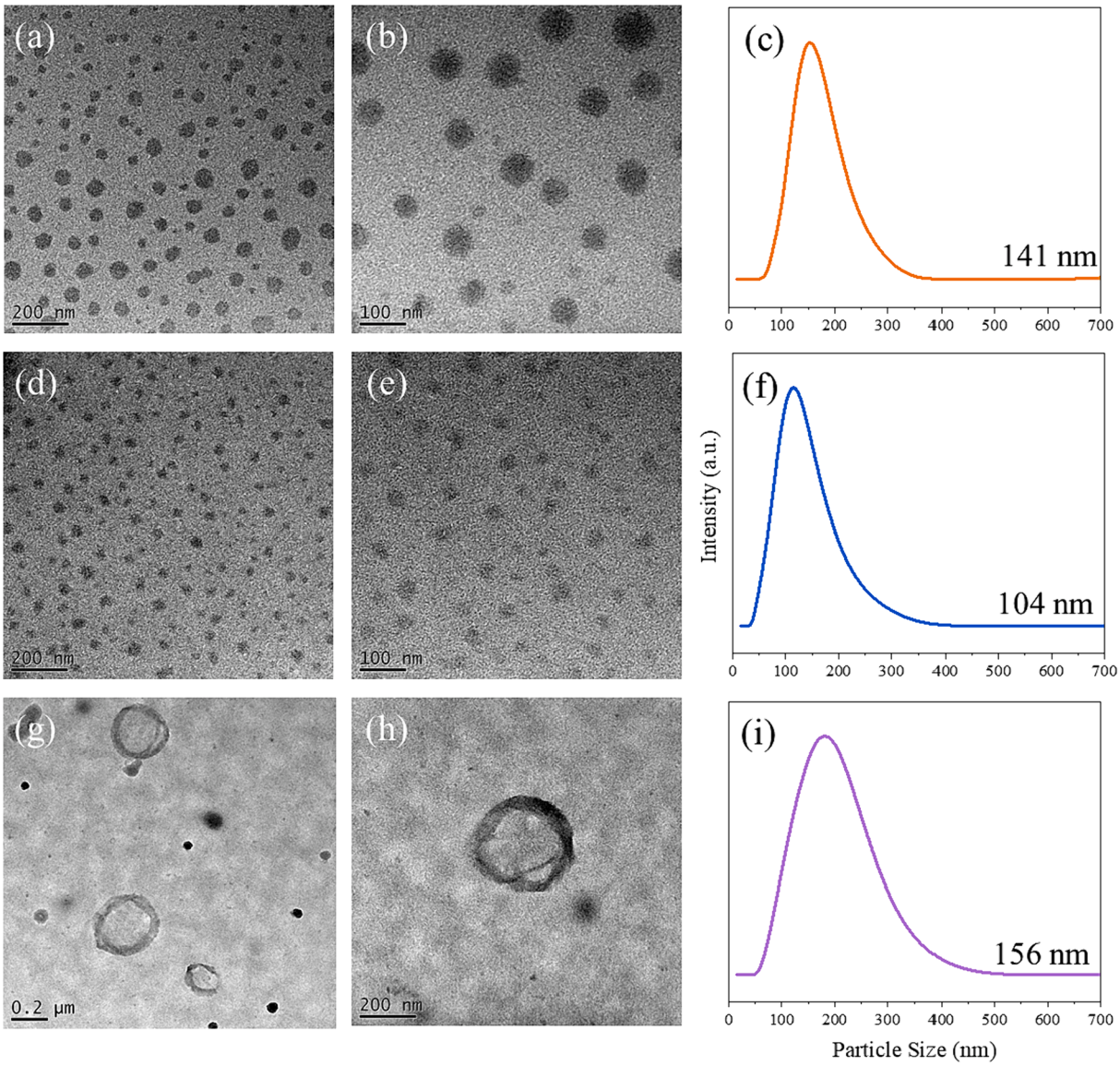

Fig. 1. (a-b) TEM images and (c) DLS analysis of HBCMs, (d-e) TEM images and (f) DLS analysis of CTPA, and (g-h) TEM images and (i) DLS analysis of HTPA. All TEM images are stained with I_2.

2.3. *The preparation of* $TPA–Br_3$ *or* $TPE–Br_4$ *cross-linked micelles (CTPA or CTPE)*

For the reinforcement of shell structures in hydrogen bonding connected micelles, $TPA–Br_3$ (5.5 mg, 0.011 mmol) or $TPE–Br_4$ (5.5 mg, 0.008 mmol) was separately introduced into micelles solutions (10 mL). The molar ratio of bromide units in $TPA–Br_3$ or $TPE–Br_4$ to pyridine units in P4VP was 2:1. The resulting mixture was slightly stirred at 60 °C for 48 hrs to accomplish the crosslinking process as depicted in Scheme 1 (b) for CTPA and Scheme 1(c) for CTPE.

2.4. *The creation of a hollow spherical structure (HTPA or HTPE)*

To induce cavitation within the cross–linked micelles, an equal volume of DMF was mixed into the micelles solution containing either CTPA or CTPE. This resulting mixture was stirred slightly overnight at room temperature and then maintained undisturbed for a week to ensure the core structure was washed completely by DMF as displayed in Scheme 1(d) for HTPA and Scheme 1(e) for HTPE.

3. Results and discussion

3.1. *Morphology of HBCMs, CTPA, HTPA, CTPE and HTPE*

In this study, we introduced two kinds of fluorescence materials, $TPA–Br_3$ and $TPE–Br_4$, as cross–linkers to stabilize the poly (S–*alt*–HPMI)/P4VP HBCMs to further achieve hollow spheres based on our previous study [24]. Fig. 1 displays TEM images and DLS analyses of HBCMs, CTPA, and HTPA based on $TPA–Br_3$ as the cross–linker. TEM images displayed the successfully self–assembled HBCMs into spherical structures successfully with diameters around 62 ± 15 nm, as displayed in Fig. 1(a-b) and Figure S1 (a), consistent with our previous findings [24]. Furthermore, the formation of cross–linked P4VP shell structure was according to the approach of Noguchi et al [40]. The process involved the utilizing bromide atoms on $TPA–Br_3$ to quaternized pyridine units and create a *p*–conjugated TPA skeleton [33] as shown in Scheme 1(b). Fig. 1(d-e) and Figure S1 (b) demonstrate that the morphologies of CTPA are still maintained spherical with diameters around 28 ± 8 nm; however, the particle size was decreased obviously. Additionally, Fig. 1(c) and Fig. 1(f) also displayed DLS analysis, suggesting

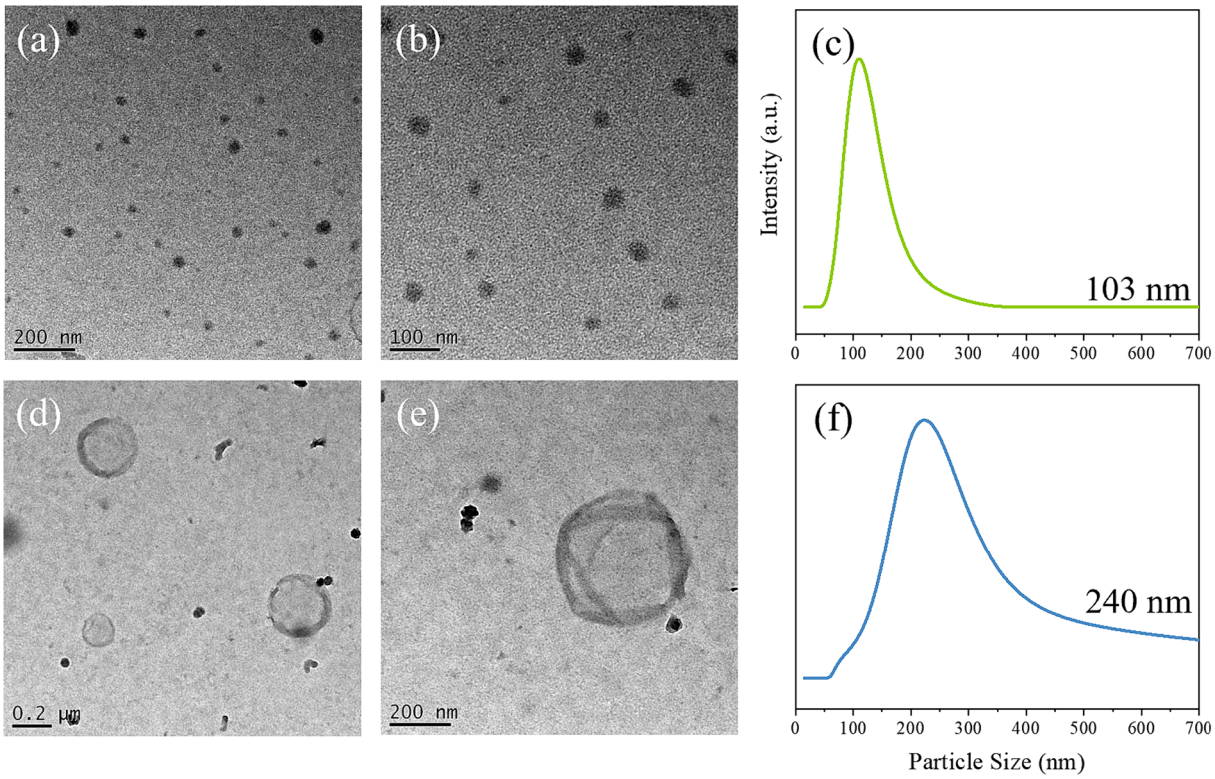

Fig. 2. (a-b) TEM images (c) DLS analysis of CTPE, and (d-e) TEM images and (f) DLS analysis of HTPE. All TEM images are stained with I_2.

that the particle size of HBCMs was shrunk from ca. 141 nm to 104 nm after cross–linking with TPA–Br_3 to form CTPA, which indicated that the P4VP shell was reinforced by TPA–Br_3 successfully. Finally, we induced cavitation in the poly(S–*alt*–HPMI) core structure in CTPA by adding DMF. Fig. 1(g-h) characterized the hollow nature of HTPA, it was obvious that higher electrons could transmit the center than the margin of the nanocage effectively, thus producing the contrast between the shell and empty center clearly [41]. Moreover, Fig. 1(i) showed that the particle size expanded to 156 nm due to the micelles solution being diluted after the DMF was added. Analogous shapes and particle sizes of the HBCMs, CTPA, and HTPA were also confirmed by AFM, as shown in Figure S2.

Fig. 2 shows TEM images and DLS analyses of HBCMs, CTPE, and HTPE, where we also utilized TPE–Br_4 to enhance the stability of HBCMs. The methodology was analogous to that of CTPA because the characterization of bromide–substituted could involve quaternization of pyridine units and created TPE framework to connect P4VP polymer chains, thereby reinforcing the shell structure as displayed in Scheme 1 (c). Fig. 2(a-b) and Figure S1 (c), reveal that CTPE also maintained spherical structures with diameters around 36 ± 10 nm after the HBCMs were cross–linked by TPE–Br_4. The DLS data reported that the particle size was decreased to 103 nm (Fig. 2(c)), which closely resembled the results for CTPA compared to Fig. 1(d)-1(f). This similarity indicated that the P4VP shell could also be cross–linked by TPE–Br_4 successfully. In the final step, we also degraded the poly(S–*alt*–HPMI) core structure in CTPE through DMF dissolution. Fig. 2(d-e) characterized the thin shells of the nanocage and the large collapsed inner cavity, which evidenced that the hollow structures of HTPE were achieved. Likewise, Fig. 2(f) reveals that the particle size was expanded to 240 nm after the micelles solution of CTPE was diluted by DMF, which was larger than HTPA. However, the distribution of particle sizes exhibited greater polydispersity. Analogous shapes and particle sizes of the HBCMs, CTPE, and HTPE were also confirmed by AFM as shown in Figure S3.

3.2. *Characterizations of* HBCMs, CTPA, HTPA, CTPE and HTPE

Hydrogen bonding connected micelles, cross-linked reaction, and core dissolution were characterized by several analytical techniques including FTIR, ^{1}H NMR, TGA, and DSC. Firstly, FTIR spectra in Fig. 3(a) and 3(d) displayed the absorption band of poly(S–*alt*–HPMI)/P4VP HBCMs at 1005 cm^{-1}, which was characteristic of the hydrogen-bonded pyridine ring, indicating that the HBCMs had been stabilized by hydrogen bonding interaction between the OH of poly(S–*alt*–HPMI) and N atom of P4VP successfully [24]. Upon cross-linked with TPA–Br_3 or TPE–Br_4, the intensity of absorption peaks around 3056 cm^{-1} (sp^2 C–H stretching) relatively increased, attributed to the aromatic rings of TPA or TPE units, the absorption bands of OH shifted to higher wavenumbers ca. 3 cm^{-1} after P4VP shell cross-linked with TPA–Br_3 and ca. 7 cm^{-1} for TPE–Br_4, indicating the formation of free OH on the poly(S–*alt*–HPMI) core due to blue shift wavenumber. Furthermore, the signals at 1005 cm^{-1} decreased, suggesting that the hydrogen-bonded N atom on the P4VP shell was replaced with cross-linked TPA–Br_3 or TPE–Br_4. Following the dissolution of the poly(S–*alt*–HPMI) core by DMF, the peaks at 1714 cm^{-1} corresponding to the symmetric C = O stretching of maleimide units in poly(S–*alt*–HPMI)) was decreased, while the peak at 1665 cm^{-1} (C = N^+ stretching) [42,43] was not apparent in this study. We observed relatively apparent signals at 1113 cm^{-1} (C-N stretching) and 620 cm^{-1} (C-Br stretching) [33] because TPA–Br_3 or TPE–Br_4 reinforced the P4VP shell structure, revealing that the collapsed of poly (S–*alt*–HPMI) core after adding DMF to form the hollow spheres. The reason for the poly(S–*alt*–HPMI) core washed out by DMF is the competition about intermolecular hydrogen bonding interaction between the OH or carbonyl in poly(S–*alt*–HPMI) with DMF compared to the OH in poly(S–*alt*–HPMI) with N atom in P4VP, which has been discussed extensively in previous study [24].

The ^{1}H NMR spectra depicted in Fig. 3(b) and 3(e) were also been investigated, and all the samples were processed in deuterated dimethyl sulfoxide (DMSO-d_6). In our previous study, we had communicated that the signals within the range of 5.8–7.8 ppm represent the protons of

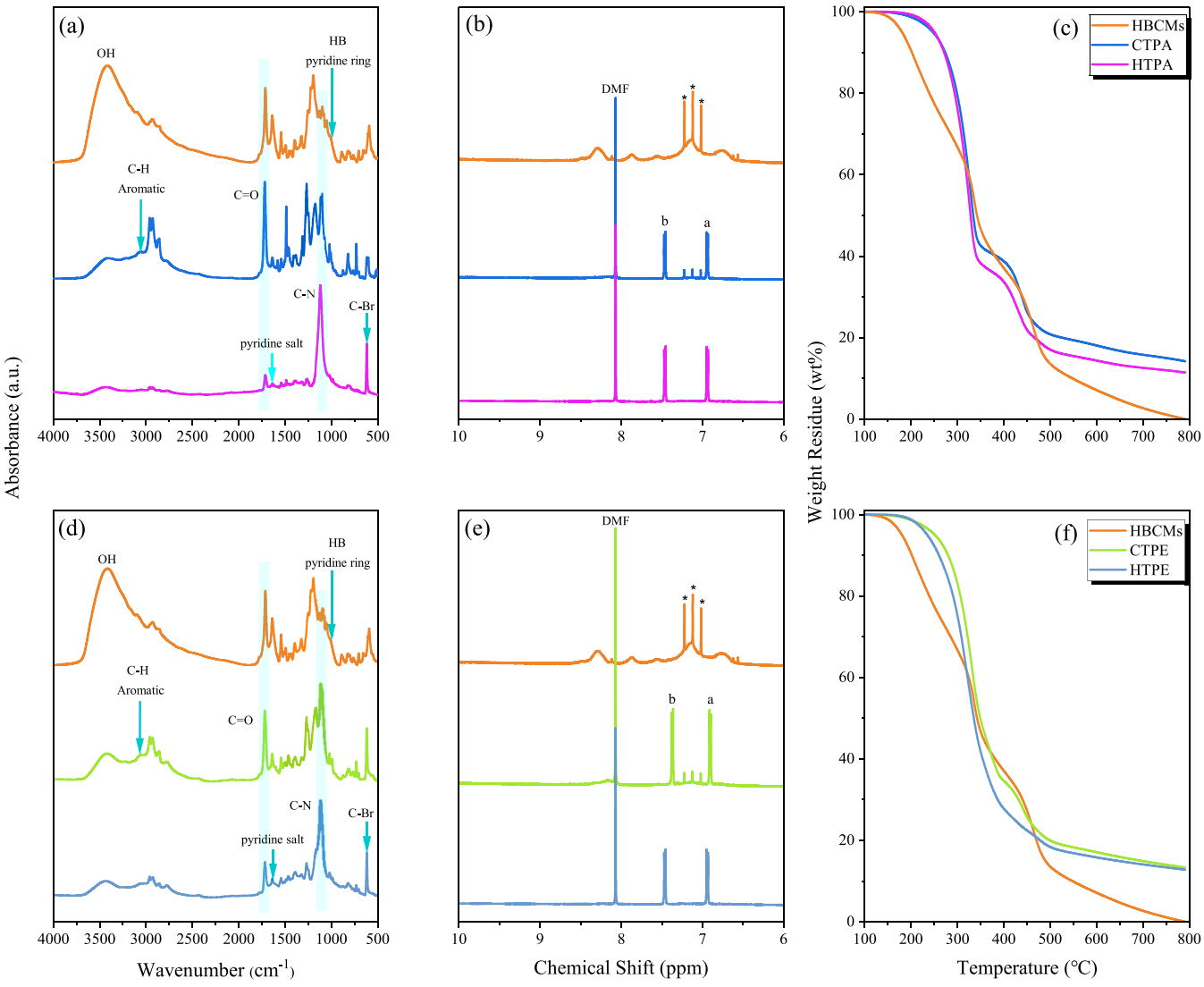

Fig. 3. (a, d) FTIR spectra, (b, e) ^{1}H NMR spectra (chloroform-*d*), and (c, f) TGA thermal analyses of HBCMs, CTPA, HTPA, CTPE and HTPE, respectively.

aromatic rings, while signals at 9.71 ppm symbolize the protons of OH units for poly(S–*alt*–HPMI) [37]; protons in pyridine ring nearby the main chain and N atom for P4VP are indicated by signals at 6.8–7.2 and 8.0–8.5 ppm [24,38]. Because the pristine poly(S–*alt*–HPMI) and P4VP could dissolve in DMSO-d_6 individually, thus the HBCMs consisting of poly(S–*alt*–HPMI)/P4VP polymer complex could move in DMSO-d_6. The signals around 6.7–7.8 and 8.2–8.4 ppm became broader and shifted downfield because of the hydrogen bonding interaction between OH and the N atom, leading the electron density around protons on aromatic and pyridine rings deshielding [44]. Remarkably, we observed three distinct signals for HBCMs (star-labeled) at 7.0, 7.1, and 7.2 ppm, indicating a unique environment for these protons. Following cross-linking with TPA–Br_3 or TPE–Br_4, all the proton signals associated with aromatic and pyridine rings vanish, and there is a notable reduction in the intensity of the three distinct signals of HBCMs (star-labeled). The observed phenomenon serves as clear evidence that the mobility of the polymer complex was constrained, implying the successful occurrence of the cross-linked reaction [45]. Furthermore, the signals at approximately 6.9 and 7.4 ppm arise from the protons associated with the aromatic rings of TPA–Br_3 or TPE–Br_4 [39], providing evidence of the successful cross-linking of the P4VP shell with TPA–Br_3 or TPE–Br_4 in HBCMs. Ultimately, the disappearance of the three distinct signals of HBCMs (star-labeled) upon the addition of DMF indicates the successful removal of the poly(S–*alt*–HPMI) core.

We also conducted the TGA analysis displayed in Fig. 3(c) and 3(f), which provided insights into the thermal behavior of the HBCMs. The thermal degradation temperatures (T_{d10}) of HMCBs comprising 69 wt% poly(S–*alt*–HPMI) and 31 wt% P4VP by weight fraction in a selective solvent mixture of THF/nitromethane was 201 ℃. The corresponding char yield at 800 ℃ was 0 wt%. Additionally, we measured the thermal characteristics of poly(S–*alt*–HPMI)/P4VP blend system with a weight fraction of 65/35 in DMF, as shown in Figure S4, indicating that the thermal stability of HBCMs was inferior to the blend system. This is because the poly(S-*alt*-HPMI)/P4VP blend system exhibits full miscibility facilitated by inter-polymer complexes, resulting in a compact structure. Conversely, the HBCMs undergo microphase separation in a selective solvent, leading to a looser structure and lower thermal stability compared to the miscible poly(S-*alt*-HPMI)/P4VP blend from a DMF solution. Furthermore, the DSC analysis displayed in Figure S5 revealed two glass transition temperatures (T_{gs}) for HBCMs, where T_{g1} was observed at 120 ℃ and.

T_{g2} was 250 ℃. Notably, these values were closely similar to the respective glass transition temperatures of pristine P4VP (T_g = 130 ℃) and poly(S–*alt*–HPMI) (T_g = 259 ℃), indicating microphase separation of HBCMs in a selective solvent. Moreover, we compared the T_g of poly (S–*alt*–HPMI)/P4VP polymer blend system, we observed that the T_{g2} of

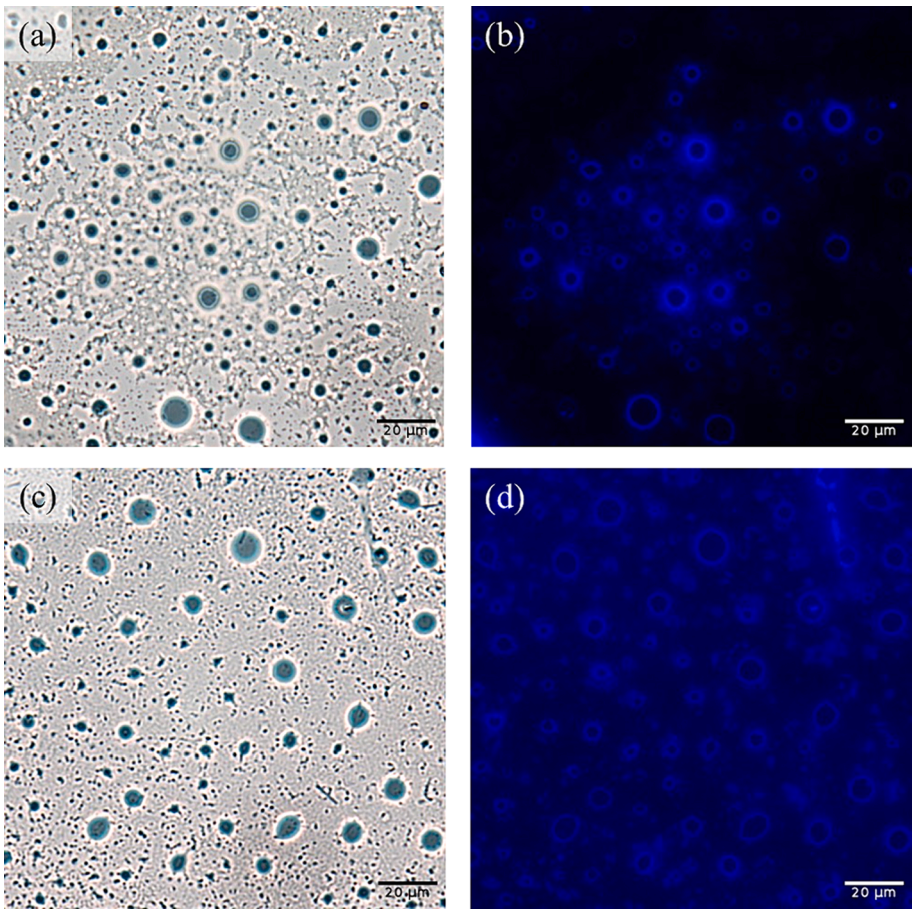

Fig. 4. Fluorescence images of CTPA with (a) optical views and (b) fluorescence views, HTPA with (c) optical views and (d) fluorescence views.

HBCMs was elevated compared to the blend system (T_g = 193 ℃). This increase can be attributed to the formation of stronger hydrogen bonding interaction between OH of poly(S–*alt*–HPMI) and N atom of P4VP in a relatively low polar selective solvent [46]. Upon cross-linking with TPA–Br_3 or TPE–Br_4, the thermal degradation temperatures (T_{d10}) of CTPA and CTPE were measured at 273 ℃ and 279 ℃, respectively. The increased temperature was attributed to chemical cross-links forming an additional framework. The cross-linking of CTPA and CTPE derived from HBCMs promotes mass retention, resulting in improved thermal stability and reinforcement of the P4VP shell. Besides, approximately 14.2 wt% and 13.3 wt% of CTPA and CTPE were observed at 800 ℃, respectively. Nevertheless, the thermal degradation temperatures (T_{d10}) of HTPA and HTPE declined to 271 ℃ and 260 ℃, respectively. This decrease was attributed to the collapse of the poly (S–*alt*–HPMI) core. The char yield of HTPA and HTPE recorded at 800 ℃ was 11.4 wt% and 12.8 wt%, respectively, indicating the residue of cross-linked P4VP shell [47–49]. These findings support the reinforcement of shell structures in HBCMs through cross-linking with TPA–Br_3 or TPE–Br_4 to form CTPA and CTPE. Subsequently, by adding DMF, the hollow spheres could be easily obtained by the solvent dissolution method.

3.3. *Optical properties of fluorescence particles*

To assess the preservation of the fluorescence properties of TPA–Br_3 or TPE–Br_4 after the cross-linked reaction, fluorescence microscopy was used to investigate the optical characteristics of CTPA, HTPA, CTPE, and HTPE. Fig. 4 depicts the optical and fluorescence images of CTPA and HTPA. In the case of TPA–Br_3 cross-linked CTPA, the prominent blue color and fluorescent signal were observed as shown in Fig. 4(b). Contrasting the optical images in Fig. 4(a), the shell structures exhibit a massive fluorescence, attributed to the conjugate system of TPA–Br_3 [50], suggesting that the P4VP chains were exclusively located surrounding the core due to the hydrogen bonding interaction and TPA–Br_3 cross-linked with P4VP shell successfully. Nonetheless, the shell structures became thinner after adding the DMF to collapse the poly (S–*alt*–HPMI) core as shown in Fig. 4(d), in comparison to Fig. 4(b). This is attributed to DMF acting as a dilute solution, causing the shell swelling [23,24]. Besides, the luminescent signal appears to diminish, likely due to the decreased density of TPA–Br_3 on the shell structures resulting from the swelling of the shell.

We also collected the optical and fluorescence images of CTPE and HTPE, as exhibited in Fig. 5. In contrast to Fig. 4, TPE–Br_4 cross-linked CTPE emits obscure green fluorescence, attributed to the well-known aggregation-induced emission (AIE) property of TPE derivatives. Specifically, Fig. 5(a) and 5(b) reveal that for TPE–Br_4 cross-linked CTPE, only micelles of a sufficiently small size are observable. This performance indicated that the density of TPE–Br_4 under these conditions was adequate for inducing aggregation and activating the restriction of intramolecular rotations (RIR) process [51–56]. Similarly, the shell structures demonstrated a reduction in thickness and luminescent intensity upon adding the DMF, as shown in Fig. 5(d). This phenomenon can be attributed to DMF acting as a dilute solution, causing the shell swelling and resulting in a decreased density of TPE–Br_4 on the shell structures. Moreover, the observation of distinct contrast between the luminescent periphery and the dark center once again confirmed the success of TPE–Br_4 cross-linked with shell structures and the formation of hollow structures.

Ultimately, we chose the most robust luminescent specimen in the bulk state, which exhibited a green color observed from the naked eye of

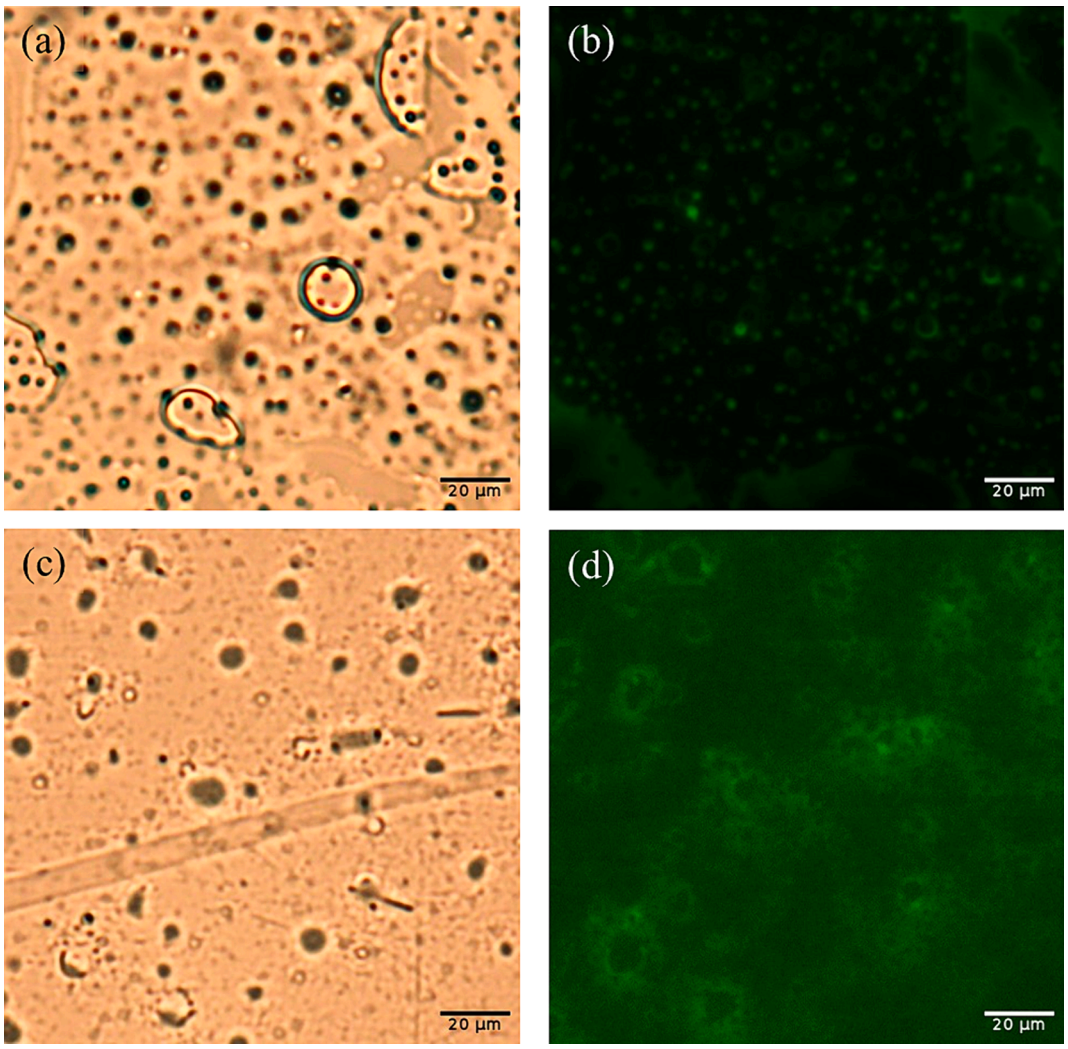

Fig. 5. Fluorescence images of CTPE with (a) optical views and (b) fluorescence views, HTPE with (c) optical views and (d) fluorescence views.

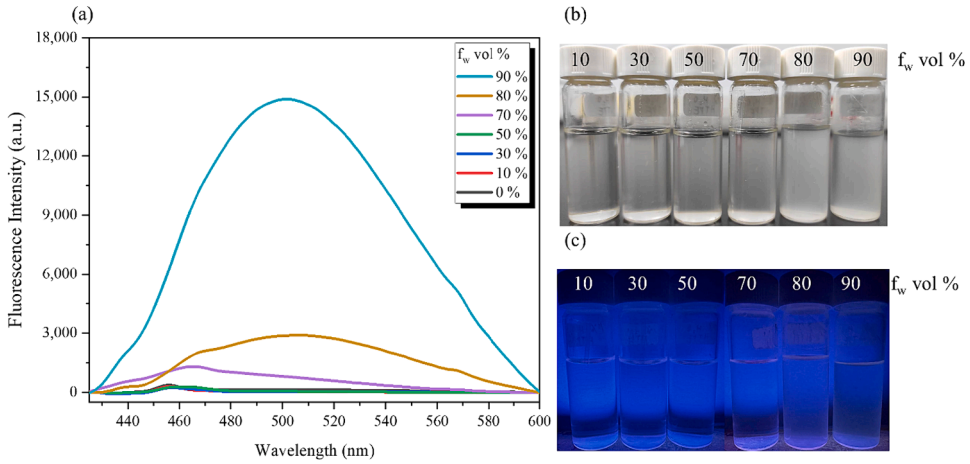

Fig. 6. HTPE solutions of (a) PL spectra, (b) photographic images under the light, (c) photographic images under the UV light with different water fractions (f_w). Fluorophore concentration: 35 μM; excitation wavelength: (a) 400 nm and (c) 254 nm.

HTPE (Figure S6) to investigate the AIE characteristics by photoluminescence (PL). For HTPE disperse in mixture solution of THF/Nitromethane/DMF (1/9/10 vol%) was non-emissive. The water as a poor solvent for HTPE was selected, thus the particles would aggregate in a water/mixture solution until the water fraction was over 70 % (f_w > 70 vol%), and the emission peak emerged. The maximum peak of HTPE with a water fraction of 90 % (f_w = 90 vol%) was 501 nm in Fig. 6(a), which was similar to some studies of TPE derivatives [32,51–56]. Besides, it was clear that the HTPE solution with a water fraction over 70 % (f_w > 70 vol%) became turbid under the light, as shown in Fig. 6(b).

Unfortunately, there was not a green color that appeared under the UV light with 365 nm, as shown in Fig. 6(c). The observation of a low quantum yield phenomenon posed challenges when attempting to measure a clear value for the photoluminescence quantum yield (PLQY) in the solution state [57].

4. Conclusion

We prepared HBCMs using poly(S-*alt*-HPMI)/ P4VP inter-polymer complexes with core/shell structures in a selective solvent. TEM images verified the formation of self-assembled spherical structures. Two kids of fluorescent, TPA–Br_3 or TPE–Br_4, were selected to act as cross-linkers for reinforcing the shell structures of HBCMs. The thermal degradation temperatures of CTPA and CTPE measured by TGA were higher than HBCMs, indicating more predominant thermal stability. To attain hollow spheres, DMF was added to remove the core structures. The morphologies, particle sizes, hydrogen bonding interaction, cross-linking reaction, core dissolution, and thermal properties were examined by TEM, AFM, DLS, FTIR, ^{1}H NMR, TGA, and DSC analyses. Furthermore, we explored the optical characteristics by utilizing a fluorescence microscope and PL analysis revealed that luminescence was observed in CTPA, HTPA, CTPE, and HTPE produced from HBCMs without the need for additional dye staining or labeling. This suggests their potential suitability for applications in nano-carriers with imaging contrast.

CRediT authorship contribution statement

Tzu-Ling Ma: Writing – original draft, Methodology, Data curation, Conceptualization. **Wei-Ting Du:** Writing – original draft, Methodology, Formal analysis, Conceptualization. **Mohamed Gamal Mohamed:** Supervision, Methodology, Conceptualization. **Shiao-Wei Kuo:** Writing – review & editing, Writing – original draft, Supervision.

Declaration of competing interest

The authors declare that they have no known competing financial interests or personal relationships that could have appeared to influence the work reported in this paper.

Data availability

The data that has been used is confidential.

Acknowledgments

This study was supported financially by the Ministry of Science and Technology, Taiwan, under contracts NSTC 110-2124-M-002-013 and 111-2223-E-110-004. The authors thank the staff at National Sun Yat-sen University for their assistance with the TEM (ID: EM022600) experiments.

Appendix A. Supplementary data

Supplementary data to this article can be found online at https://doi.org/10.1016/j.eurpolymj.2024.112954.

References

[1] Y. Zhang, P. Wang, N. Li, C. Guo, S. Li, The effect of topology on block Copolymer Nanoparticles: Linear versus Star block Copolymers in toluene, Polymers 14 (2022) 3691, https://doi.org/10.3390/polym14173691.
[2] S.W. Kuo, Hydrogen bond-mediated self-assembly and supramolecular structures of diblock copolymer mixtures, Eur. Polym. J. 58 (2009) 455–464, https://doi.org/10.1002/pi.2513.
[3] K. Lee, B.H. Sohn, Step-growth polymerization of supracolloidal chains from patchy micelles of diblock copolymers, J. Colloid Interface Sci. 648 (2023) 727–735, https://doi.org/10.1016/j.jcis.2023.06.031.
[4] P.C. Li, Y.C. Lin, M. Chen, S.W. Kuo, Self-assembled structures from PEGylated polypeptide block copolymers synthesized using a combination of ATRP, ROP, and click chemistry, Soft Matter 9 (2013) 11257–11269, https://doi.org/10.1039/C3SM52061G.
[5] A. Noel, Y.P. Borguet, K.L. Wooley, Self-reporting degradable fluorescent grafted copolymer micelles derived from biorenewable resources, ACS Macro Lett. 4 (2015) 645–650, https://doi.org/10.1021/acsmacrolett.5b00227.
[6] L. Atanase, J. Desbrieres, G. Riess, Micellization of synthetic and polysaccharides-based graft copolymers in aqueous media, Prog. Polym. Sci. 73 (2017) 32–60, https://doi.org/10.1016/j.progpolymsci.2017.06.001.
[7] J. Li, Z. Li, T. Zhou, J. Zhang, H. Xia, H. Li, J. He, S. He, L. Wang, Positively charged micelles based on a triblock copolymer demonstrate enhanced corneal penetration, Int. J. Nanomedicine 10 (2015) 6027–6037, https://doi.org/10.2147/IJN.S90347.
[8] D. Kim, H. Matsuoka, Y. Saruwatari, Formation of sulfobetaine-containing entirely ionic PIC (polyion complex) micelles and their temperature responsivity, Langmuir 36 (2020) 10130–10137, https://doi.org/10.1021/acs.langmuir.0c01577.
[9] Q. Lin, C.C. Lim, C. Owh, J.H.M. Wong, V. Ow, B. Sim, Y.J. Boo, M.P. Yew, Y. H. Leow, L. Guo, PEG-free pH-responsive thermogels containing amphiphilic polycationic polyethylenimine Copolymers, Macromolecules 56 (2023) 9368–9378, https://doi.org/10.1021/acs.macromol.3c01600.
[10] S. Perumal, R. Atchudan, W. Lee, A review of polymeric micelles and their applications, Polymers 14 (2022) 2510, https://doi.org/10.3390/polym14122510.
[11] Y. Han, N. Liang, P. Yan, Y. Kawashima, F. Cui, S. Sun, A chitosan-based micellar system as nanocarrier for the delivery of paclitaxel, Polymers 12 (2020) 380, https://doi.org/10.3390/polym12020380.
[12] Q. Liu, F. Li, N. Ji, L. Dai, L. Xiong, Q. Sun, Acetylated debranched starch micelles as a promising nanocarrier for curcumin, Food Hydrocoll. 111 (2021) 106253, https://doi.org/10.1016/j.foodhyd.2020.106253.
[13] Y. Zhao, C. Fang, G. Zhang, D. Hubble, A. Nallapaneni, C. Zhu, Z. Zhao, Z. Liu, J. Lau, Y. Fu, A micelles electrolyte enabled by fluorinated ether additives for polysulfide suppression and li metal stabilization in li-S battery, Front. Chem. 8 (2020) 484, https://doi.org/10.3389/fchem.2020.00484.
[14] S. Rathod, A. Joshi, D. Ray, V.K. Aswal, G. Verma, P. Bahadur, S. Tiwari, Changes in aggregation properties of TPGS micelles in the presence of sodium cholate, Colloids Surf. a: Physicochem. Eng. 610 (2021) 125938, https://doi.org/10.1016/j.colsurfa.2020.125938.
[15] M.G. Mohamed, S.W. Kuo, Progress in the self-assembly of organic/inorganic polyhedral oligomeric silsesquioxane (POSS) hybrids, Soft Matter 18 (2022) 5535–5561, https://doi.org/10.1039/D2SM00635A.
[16] T.C. Chou, W.C. Chen, M.G. Mohamed, Y.C. Huang, S.W. Kuo, Organic-inorganic Phenolic/POSS hybrids provide highly ordered mesoporous structures templated by high thermal stability of PS-b-P4VP diblock Copolymer, Chem. Eur. J. 29 (2023) e202300538.
[17] K. Kuperkar, D. Patel, L.I. Atanase, P. Bahadur, Amphiphilic block copolymers: their structures, and self-assembly to polymeric micelles and polymersomes as drug delivery vehicles, Polymers 14 (2022) 4702, https://doi.org/10.3390/polym14214702.
[18] D. Hwang, J.D. Ramsey, A.V. Kabanov, Polymeric micelles for the delivery of poorly soluble drugs: from nanoformulation to clinical approval, Adv. Drug Deliv. Rev. 156 (156) (2020) 80–118, https://doi.org/10.1016/j.addr.2020.09.009.
[19] Y. Cai, J. Qi, Y. Lu, H. He, W. Wu, The in vivo fate of polymeric micelles, Adv. Drug Deliv. Rev. 188 (2022) 114463, https://doi.org/10.1016/j.addr.2022.114463.
[20] M. Guo, M. Jiang, Non-covalently connected micelles (NCCMs): the origins and development of a new concept, Soft Matter 495 (2009) 495–500, https://doi.org/10.1039/b813556h.
[21] J. Wang, M. Jiang, Polymeric self-assembly into micelles and hollow spheres with multiscale cavities driven by inclusion complexation, J. Am. Chem. Soc. 128 (2006) 3703–3708, https://doi.org/10.1021/ja056775v.
[22] Y.C. Wu, Y.S. Wu, S.W. Kuo, Bioinspired photo-Core-crosslinked and noncovalently connected micelles from functionalized polystyrene and poly (ethylene oxide) Homopolymers, Macromol. Chem. Phys. 214 (2013) 563–571, https://doi.org/10.1002/macp.201200648.
[23] M. Wang, M. Jiang, F. Ning, D. Chen, S. Liu, H. Duan, Block-copolymer-free strategy for preparing micelles and hollow spheres: self-assembly of poly (4-vinylpyridine) and modified polystyrene, Macromolecules 35 (2002) 5980–5989, https://doi.org/10.1021/ma0201330.
[24] T.L. Ma, W.T. Du, S.W. Kuo, Construction of micelles and hollow spheres via the self-assembly behavior of poly (styrene-alt-pHPMI) copolymers with poly (4-vinylpyridine) derivatives mediated by hydrogen bonding interactions, Soft Matter 19 (2023) 4706–4716, https://doi.org/10.1039/D3SM00595J.
[25] H. Lee, K. Char, Morphological changes from silica tubules to hollow spheres controlled by the Intermolecular Interactions within block Copolymer micelles templates, ACS Appl. Mater. Interfaces 1 (2009) 913–920, https://doi.org/10.1021/am900026s.
[26] D.H. Kim, D.W. Kim, J.Y. Jang, N. Lee, Y.J. Ko, S.M. Lee, H.J. Kim, K. Na, S.U. Son, Fe_3O_4@ void@ microporous organic polymer-based multifunctional drug delivery systems: targeting, imaging, and magneto-thermal behaviors, ACS Appl. Mater. Interfaces 12 (2020) 37628–37636, https://doi.org/10.1021/acsami.0c12237.
[27] B. Ghosh, S. Biswas, Polymeric micelles in cancer therapy: state of the art, J. Control. Release 332 (2021) 127–147, https://doi.org/10.1016/j.jconrel.2021.02.016.
[28] D. Maysinger, J. Lovrić, A. Eisenberg, R. Savić, Fate of micelles and quantum dots in cells, Eur. J. Pharm. Biopharm. 65 (2007) 270–281, https://doi.org/10.1016/j.ejpb.2006.08.011.

[29] J. van Wijk, N. van Deventer, E. Harmzen, J. Meuldijk, B. Klumperman, Formation of hybrid poly (styrene-co-maleic anhydride)–silica microcapsules, J. Mater. Chem. B 2 (2014) 4826–4835, https://doi.org/10.1039/c4tb00473f.
[30] S. Razzaque, Y. Cheng, I. Hussain, B. Tan, Synthesis of surface functionalized hollow microporous organic capsules for doxorubicin delivery to cancer cells, Polym. Chem. 11 (11) (2020) 2110–2118, https://doi.org/10.1039/c9py01772k.
[31] S.Y. Chang, A.M. Elewa, M.G. Mohamed, I.M.A. Mekhemer, M.M. Samy, K. Zhang, H.H. Chou, S.W. Kuo, Rational design and synthesis of bifunctional dibenzo[g, p] chrysene-based conjugated microporous polymers for energy storage and visible light-driven photocatalytic hydrogen evolution, Mater. Today. Chem. 33 (2023) 101680, https://doi.org/10.1016/j.mtchem.2023.101680.
[32] M.G. Mohamed M.H. Elsayed A.M. Elewa A.F.M. EL-Mahdy, C.H. Yang, A.A. Mohammed, H.H. Chou, S.W. Kuo, Pyrene-containing conjugated organic microporous polymers for photocatalytic hydrogen evolution from water Catal. Sci. Technol. 11 2021 2229 2241 10.1039/d0cy02482a.
[33] A.O. Mousa, Z.I. Lin, C.H. Chuang, C.K. Chen, S.W. Kuo, M.G. Mohamed, Rational Design of Bifunctional Microporous Organic Polymers Containing Anthracene and Triphenylamine Units for energy storage and biological applications, Int. J. Mol. Sci. 24 (2023) 8966, https://doi.org/10.3390/ijms24108966.
[34] M.G. Mohamed, H.Y. Hu, S. Santhoshkumar, M. Madhu, T.H. Mansoure, C. W. Hsiao, Y. Ye, C.W. Huang, W.L. Tseng, S.W. Kuo, Design and synthesis of bifunctional conjugated microporous polymers containing tetraphenylethene and bisulfone units for energy storage and fluorescent sensing of p-nitrophenol, Colloids Surf. a: Physicochem. Eng. 680 (2024) 132675, https://doi.org/10.1016/j.colsurfa.2023.132675.
[35] C.W.T. Leung, Y. Hong, S. Chen, E. Zhao, J.W.Y. Lam, B.Z. Tang, A photostable AIE luminogen for specific mitochondrial imaging and tracking, J. Am. Chem. Soc. 135 (2013) 62–65, https://doi.org/10.1021/ja310324q.
[36] B. Kulkarni, S. Qutub, V. Ladelta, N.M. Khashab, N. Hadjichristidis, AIE-based fluorescent triblock copolymer micelles for simultaneous drug delivery and intracellular imaging, Biomacromolecules 22 (2021) 5243–5255, https://doi.org/10.1021/acs.biomac.1c01165.
[37] W.T. Du, E.A. Orabi, M.G. Mohamed, S.W. Kuo, Inter/intramolecular hydrogen bonding mediate miscible blend formation between near-perfect alternating poly (styrene-alt-hydroxyphenylmaleimide) copolymers and poly (vinyl pyrrolidone), Polymer 219 (2021) 123542, https://doi.org/10.1016/j.polymer.2021.123542.
[38] W.T. Du, T.L. Ma, S.W. Kuo, Steric hindrance affects interactions of poly (styrene–alt–DMHPMI) copolymer with strongly hydrogen-bond-accepting homopolymers, Polymer 268 (2023) 125694, https://doi.org/10.1016/j.polymer.2023.125694.
[39] A.O. Mousa, M.G. Mohamed, Z.I. Lin, C.H. Chuang, C.K. Chen, S.W. Kuo, Conjugated microporous polymers as a novel generation of drug carriers: a systemic study toward efficient carriers of tetracycline antibiotic, Eur. Polym. J. 196 (2023) 112254, https://doi.org/10.1016/j.eurpolymj.2023.112254.
[40] J.M. Fréchet, M.V. de Meftahi, Poly (vinyl pyridine) s: simple reactive polymers with multiple applications, Br. Polym. J. 16 (1984) 193–198, https://doi.org/10.1002/pi.4980160407.
[41] X. Yuan, M. Jiang, H. Zhao, M. Wang, Y. Zhao, C. Wu, Noncovalently connected polymeric micelles in aqueous medium, Langmuir 17 (2001) 6122–6126, https://doi.org/10.1021/la010574x.
[42] Y.M. Lam, L. Song, Y.C. Moy, L. Xi, C. Boothroyd, Controlled chemical stabilization of self-assembled PS-P4VP nanostructures, J. Colloid Interface Sci. 317 (2008) 255–263, https://doi.org/10.1016/j.jcis.2007.09.044.
[43] G. Zhang, S. Tang, A. Li, L. Zhu, Thermally stable metallic nanoparticles prepared via core-cross-linked block copolymer micellar nanoreactors, Langmuir 33 (2017) 6353–6362, https://doi.org/10.1021/acs.langmuir.7b00573.
[44] R. Narayan, P. Kumar, K. Narayan, S. Asha, Nanostructured crystalline comb Polymer of perylenebisimide by directed self-assembly: poly (4-vinylpyridine)-pentadecylphenol perylenebisimide, Adv. Funct. Mater. 23 (2013) 2033–2043, https://doi.org/10.1002/adfm.201202366.
[45] M. Roy, P.R. Rajamohanan, S. Ravindranathan, A. sk,, Self-assembly of bispentadecylphenol substituted perylenediimide with PS-b-P4VP for structure-property insight into the Core of Core-Shell micelles, ACS Appl. Polym. Mater. 2 (2020) 805–816, https://doi.org/10.1021/acsapm.9b01099.
[46] S.W. Kuo, Hydrogen bonding in polymeric materials, John Wiley & Sons (2018), https://doi.org/10.1002/9783527804276.
[47] X. Wang, K. Liu, A.C. Arsenault, D.A. Rider, G.A. Ozin, M.A. Winnik, I. Manners, Shell-cross-linked cylindrical polyisoprene-b-polyferrocenylsilane (PI-b-PFS) block copolymer micelles: one-dimensional (1D) organometallic nanocylinders, J. Am. Chem. Soc. 129 (2007) 5630–5639, https://doi.org/10.1021/ja068730f.
[48] J. Park, S.J. Smith, C.D. Wood, X. Mulet, M. Seo, Core hyper-cross-linked star polymers from block polymer micelles precursors, Polym. Chem. 11 (2020) 7178–7184, https://doi.org/10.1039/D0PY01225D.
[49] A. Sethi M. Ahmad T. Huma I. Khalid I. Ahmad Evaluation of low molecular weight cross linked chitosan nanoparticles, to enhance the bioavailability of 5-flourouracil Dose Response 19 2021 15593258211025353 10.1177/15593258211025353.
[50] D. Li, P. Zhou, Y. Hu, G. Li, L. Xia, Rapid determination of illegally added Sudan I in cake by triphenylamine functionalized polyhedral oligomeric silsesquioxane fluorescence sensor, Spectrochim. Acta A Mol. Biomol. Spectrosc. 282 (2022) 121673, https://doi.org/10.1016/j.saa.2022.121673.
[51] N.W. Tseng, J. Liu, J.C. Ng, J.W. Lam, H.H. Sung, I.D. Williams, B.Z. Tang, Deciphering mechanism of aggregation-induced emission (AIE): is E-Z isomerisation involved in an AIE process? Chem. Sci. 3 (2012) 493–497, https://doi.org/10.1039/C1SC00690H.
[52] R. Hu, J.L. Maldonado, M. Rodriguez, C. Deng, C.K. Jim, J.W. Lam, M.M. Yuen, G. Ramos-Ortiz, B.Z. Tang, Luminogenic materials constructed from tetraphenylethene building blocks: synthesis, aggregation-induced emission, two-photon absorption, light refraction, and explosive detection, J. Mater. Chem. a. 22 (22) (2012) 232–240, https://doi.org/10.1039/C1JM13556B.
[53] L.C. Chou, M.G. Mohamed, S.W. Kuo, Y. Nakamura, C.F. Huang, Synthesis of multifunctional poly(carbamoyl ester)s containing dual-cleavable linkages and an AIE luminogen via passerini-type multicomponent polymerization, Chem. Commun. 58 (2022) 12317–12320, https://doi.org/10.1039/D2CC03829C.
[54] C.H. Chiang, M.G. Mohamed, W.C. Chen, M. Madhu, W.L. Tseng, S.W. Kuo, Construction of fluorescent conjugated polytriazole containing double-Decker silsesquioxane: click Polymerization and thermal stability, Polymers 15 (2023) 331, https://doi.org/10.3390/polym15020331.
[55] M.G. Mohamed, K.C. Hsu, J.L. Hong, S.W. Kuo, Unexpected fluorescence from maleimide-containing polyhedral oligomeric silsesquioxanes: nanoparticle and sequence distribution analyses of polystyrene-based alternating copolymers, Polym. Chem. 7 (2016) 135–145, https://doi.org/10.1039/C5PY01537E.
[56] M.G. Mohamed, F.H. Lu, J.L. Hong, S.W. Kuo, Strong emission of 2,4,6-triphenyl-pyridine-functionalized polytyrosine and hydrogen-bonding interactions with poly (4-vinylpyridine), Polym. Chem. 6 (2015) 6340–6350, https://doi.org/10.1039/C5PY00938C.
[57] H. Kwon, S. Park, S. Kang, H. Lee, J. Park, Three-color white photoluminescence emission using perovskite nanoplatelets and organic emitter, Molecules 27 (2022) 3982, https://doi.org/10.3390/molecules27133982.